Synthesis and investigation of novel sulfonamide-1,2,3-triazoles corrosion inhibitors for E24 steel in 1 M HCl solution: A combination of modeling and experimental approaches

M. Errili,[1]* K. Tassaoui,[1] A. Chraka,[2] M. Damej,[1] H.T. Rahal,[3] N. Labjar,[4] A. El Mahmoudi,[5] K. Bougrin,[5] A. Berisha[6] and M. Benmessaoud[1]

[1]CERNE2D, Energy, Materials and Sustainable Development Team, Higher School of Technology Sale, Mohammed V University in Rabat 8007, Morocco
[2]Laboratory of Materials Engineering and Sustainable Energy (IMED-LAB), Faculty of Science, Abdelmalek Essaadi University, Tetouan 2117, Morocco
[3]Department of Chemistry, Faculty of Science, Lebanese International University, PO Box: 146404, Lebanon
[4]CERNE2D, LS3MNE2, ENSAM, Mohammed V University in Rabat10100, Morocco
[5]Laboratory of Plant Chemistry and Organic and Bioorganic Synthesis, URAC23, Faculty of Science, Geophysics, Natural Patrimony and Green Chemistry (GEOPAC) Research Center, Mohammed V University in Rabat, PO Box 1014, 10000, Rabat, Morocco
[6]Department of Chemistry, Faculty of Natural and Mathematics Science, University of Prishtina, 10000 Prishtina, Kosovo
**E-mail: milouderrili@gmail.com*

Abstract

Carbon steel is widely employed across various industrial sectors due to its advantageous properties. However, corrosion remains a significant issue, particularly in acidic environments. In this study, we employed two novel organic compounds: 2-(propylaminecarbonyl)-*N*-((1-(benzyl)-1*H*-1,2,3-triazol-4-yl)methyl)benzenesulfonamide (BTMB) and 2-((1-(4-bromophenyl)-1*H*-1,2,3-triazol-4-yl)methyl)benzo[*d*]isothiazol-3(2*H*)-one 1,1-dioxide (BPMS). These compounds were evaluated for the first time as corrosion inhibitors for E24 steel in a 1 M HCl solution. The inhibitory performance of BTMB and BPMS was assessed using various electrochemical techniques coupled with computational chemistry approaches. Potentiodynamic polarization (PDP) curve data revealed that the inhibition efficiency of both BTMB and BPMS increases with concentration, reaching maximum efficiencies of 92.33% and 89.37%, respectively, at 1 mM concentration. Additionally, the PDP curves indicated that BTMB and BPMS act as mixed-type inhibitors. Both inhibitors demonstrated significant efficacy across a broad temperature range (293–323 K). The adsorption behavior of these inhibitors on the E24 steel surface adhered to the Langmuir adsorption isotherm. To elucidate the experimental findings at the electronic and atomic scales, computational studies were

conducted using density functional theory (DFT), Monte Carlo (MC) simulations, and molecular dynamics (MD) simulations.

Received: May 28, 2024. Published: July 23, 2024 doi: 10.17675/2305-6894-2024-13-3-14

Keywords: *BTMB/BPMS, corrosion inhibitors, E24 steel, electrochemical techniques, computational investigations.*

1. Introduction

One of the primary challenges faced by industrialized nations is the phenomenon of metal corrosion [1]. In various industrial applications, such as metal pickling, chemical treatments, and sedimentation removal, acidic media like hydrochloric acid are commonly used [2]. Despite its widespread use, E24 steel exhibits poor resistance to corrosion when exposed to hydrochloric acid solutions [3].This results in the production of significant amounts of waste annually due to the aggressive nature of the acidic medium, which accelerates metal corrosion [4]. Therefore, identifying a suitable solution to mitigate this issue is crucial [5]. A cost-effective and efficient method for protecting metals involves the use of synthetic organic corrosion inhibitors [6]. The effectiveness of these inhibitors is largely dependent on their functional groups, which enable them to adhere to the metal surface. Most effective organic inhibitors contain heterocyclic rings and atoms such as oxygen, sulfur, and nitrogen, along with conjugated double bonds that collectively facilitate their adsorption onto the metal surface [7]. These inhibitors function by creating a barrier layer that isolates the corrosive medium [8], a process that often involves chemical, physical, or mixed adsorption mechanisms [9]. Recently, computational chemistry has gained prominence in various branches of chemistry, including the study of corrosion inhibitors. It has proven to be a powerful tool for understanding the mechanisms of inhibitors and their interactions with metal surfaces [10]. In particular, Density Functional Theory (DFT) has demonstrated its ability to accurately predict molecular geometric properties, binding energies, and the interactions between inhibitors and metal surfaces [11]. However, to achieve a more precise and comprehensive understanding of these empirical phenomena, atomic-scale modeling methods such as molecular dynamics (MD) and Monte Carlo (MC) simulations are also essential [12].This study aims to evaluate the effectiveness of two inhibitors, BTMB and BPMS, in preventing the corrosion of E24 steel in a solution containing 1 M hydrochloric acid (HCl). The evaluation was conducted using both stationary and transient electrochemical methods. Additionally, a thorough investigation was performed to assess the impact of inhibitor concentration and temperature. Theoretical calculations, including DFT, MC, and MD, were employed to validate the findings. These calculations are frequently used to identify the relevant adsorption sites of the inhibitors by providing a comprehensive understanding of their geometry and adsorption energy on the metal surface at a molecular scale.

2. Experimental

2.1. BTMB and BPMS synthesis

2.1.1. The synthesis procedure for 2-(propylaminecarbonyl)-N-((1-(benzyl)-1H-1,2,3-triazol-4yl)methyl) benzenesulfonamide (BTMB)

The procedure for creating BTMB (5) (Figure 1) is as follows: *N*-propargyl saccharin (1) (1 mmol), benzyl chloride (2) ($1 \cdot 10^{-3}$ mol), NaN_3 (3) ($1.2 \cdot 10^{-3}$ mol), and propyl amine (4) ($2 \cdot 10^{-3}$ mol) were placed in a pressure closed-vial with Ag_3PO_4–MEA (10 wt.%) and 10 mL water. Next, the blend underwent irradiation for 20 minutes at 80°C, utilizing a microwave digestion system capable of reaching a maximum power of 1600 W. The reaction's completion was confirmed using TLC (thin-layer chromatography Following completion, the solid catalyst was retrieved *via* filtration, while the reaction mixture underwent extraction using DCM (3·10 mL). The amalgamated organic layer was then rinsed with a 1 N HCl acidic solution (2×0.015 L), dried using anhydrous $MgSO_4$, and concentrated using a vacuum. After undergoing recrystallization in Ethanol, the target product (5) was obtained through additional purification [13].

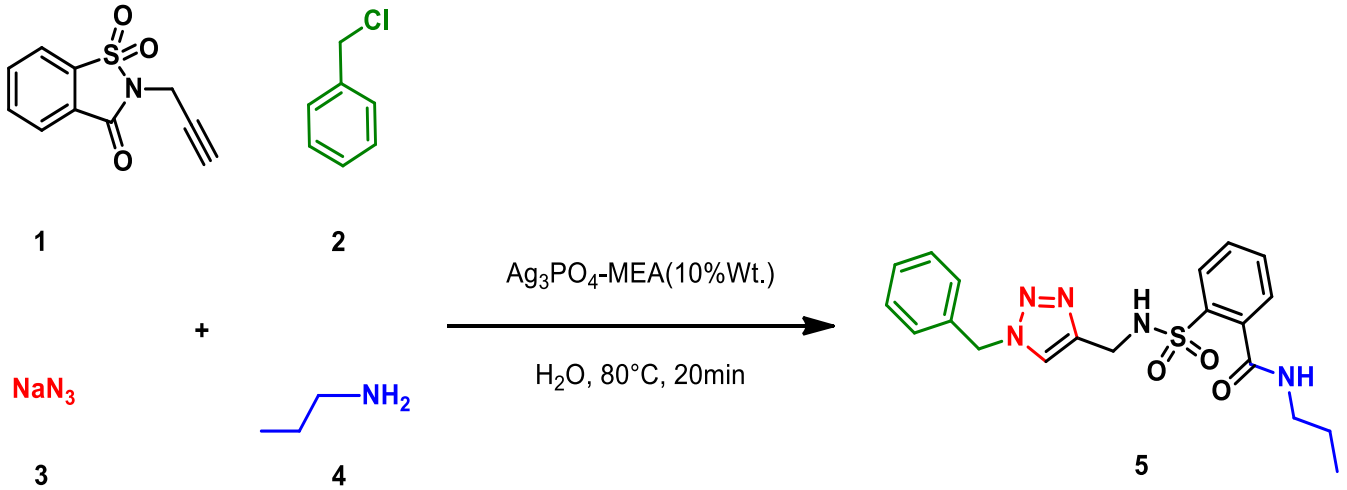

Figure 1. The procedure for creating of BTMB.

This passage describes the synthesis and characterization of BTMB (compound 5). The product is a yellow viscous oil with an 84% yield. The compound was analyzed by TLC, which revealed an R_f value of 0.48 using a solvent mixture of cyclohexane and AcOEt (2/8, v/v). DMSO-d6 was used as a solvent to obtain the nuclear magnetic resonance (NMR) spectra of the compound. The spectra showed characteristic peaks at δ 8.69 (t, J=5.7 Hz, 1H), 7.84 (s, 1H), 7.78 (dd, J=7.9, 1.2 Hz, 1H), 7.60 (td, J=7.5, 1.3 Hz, 1H), 7.51 (td, J=7.7, 1.4 Hz, 1H), 7.45–7.39 (m, 2H), 7.35–7.25 (m, 3H), 7.19 (d, J=6.3 Hz, 2H), 5.44 (s, 2H), 4.10 (d, J=6.0 Hz, 2H), 3.15 (t, J=7.1, 5.8 Hz, 2H), 1.54–1.43 (m, 2H), 0.86 (t, J=7.4 Hz, 3H). The peaks observed in the carbon-13 NMR (^{13}C NMR) spectra include signals at δ 168.9, 144.0, 137.7, 136.4, 136.3, 133.1, 130.3, 129.7, 129.3 (2C), 128.9, 128.7,

128.5 (2C), 123.8, 53.2, 41.6, 38.9, 22.5, and 11.9, which are characteristic of the compound under investigation. The mass spectrometry (MS) analysis showed an ion with a mass-to-charge ratio (*m/z*) of 412.1 $[M+H]^+$ in the electrospray ionization positive mode (ESI^+).

2.1.2. The synthesis procedure for 2-((1-(4-bromophenyl)-1H-1,2,3-triazol-4-yl)methyl)-benzo[d]isothiazol-3(2H)-one 1,1-dioxide (BPMS)

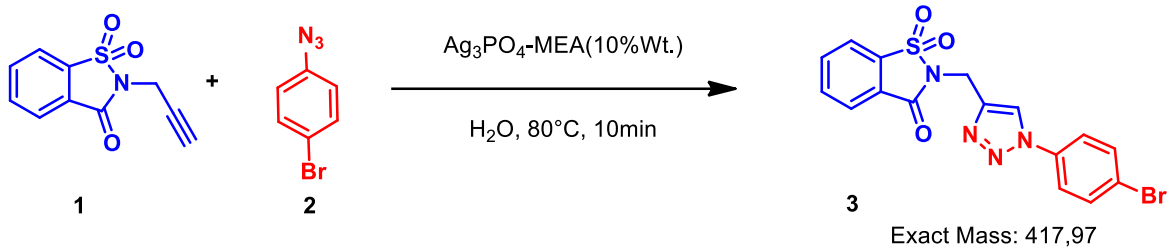

1 2 3

Figure 2. The procedure for creating of (BPMS).

The compound (BPMS) (3) was obtained as a white solid with a yield of 86%. Its R_f value in TLC, employing a solvent mixture of cyclohexane and acetone ethyl acetate (2:8, v/v), was determined to be 0.5. The compound's proton NMR spectrum, recorded at 400 MHz in DMSO, showed signals at δ 8.88 (s, 1H), 8.35 (d, J=7.6 Hz, 1H), 8.17 (d, J=7.5 Hz, 1H), 8.11–8.00 (m, 2H), 7.89 (d, J=8.8 Hz, 2H), 7.80 (d, J=8.8 Hz, 2H), and 5.10 (s, 2H). The carbon NMR spectrum, recorded at 101 MHz in DMSO, showed signals at δ 157.8, 142.2, 136.4, 135.4, 135.1, 134.8, 132.3 (2C), 125.8, 124.7, 121.7, 121.4 (2C), 121.1, 120.9, and 32.9. The mass spectrum in ESI^+ mode exhibited a peak at *m/z* 420.9 $[M+H]^+$ for the compound.

2.2. Metal chemical composition and corrosive solution preparation

Table 1 presents the chemical composition of E24 steel employed in this study. Corrosive test solutions were formulated by diluting analytical grade concentrated hydrochloric acid (37%) with distilled water. Inhibitor concentrations were varied from 0.05 mM to 1 mM for the experiments.

Table 1. Composition of E24 steel.

Compositions	C	Si	Mn	Cr	P	S	Ti	Co	Fe
(wt.%)	0.11	0.24	0.47	0.077	0.021	0.016	0.011	0.009	99.046

2.3. Electrochemical techniques

In our study, electrochemical experiments were conducted using a PGZ-100 potentiostat managed by the Volta Master software. We utilized a three-electrode cell configuration: an E24 steel working electrode (WE), a platinum counter electrode (CE), and a saturated calomel electrode (SCE) serving as the reference electrode. Prior to performing polarization

and electrochemical impedance spectroscopy (EIS) measurements, the working electrode was stabilized to reach the open-circuit potential (OCP) in the test solution. Polarization curves were acquired by scanning from –0.8 V to –0.1 V at a rate of 1 mV/s relative to the OCP. EIS was carried out over a frequency range from 100 kHz to 10 mHz, and the resulting data were displayed on Nyquist plots. Analysis of the experimental data was conducted using the EC-Lab software. The inhibition efficiency (*IE*%) was calculated using specific equations provided in the study [14]:

$$IE\% = \frac{i_{corr}^{0} - i_{corr}^{inh}}{i_{corr}^{0}} \cdot 100 \quad (1)$$

Where i_{corr}^{0} and i_{corr}^{inh} represent the corrosion current density without and with inhibitor respectively.

$$IE\% = \frac{R_{ct}^{inh} - R_{ct}^{0}}{R_{ct}^{inh}} \cdot 100 \quad (2)$$

Where R_{ct}^{inh} and R_{ct}^{0} represent the charge transfer resistance respectively with and without inhibitor.

2.4. Quantum chemical calculations

The quantum chemical modeling results were obtained using the Dmol3 module within the Materials Studio program [15] Calculations were conducted for inhibitor molecules in both neutral and protonated states employing the M-06L exchange-correlation function and the DNP basis set with polarization [16]. The aqueous phase was simulated using the COSMO model [17]. Vibrational analysis confirmed the minimum point as the lowest energy point on the potential energy surface [18]. DFT was employed to compute electronic structure properties, including the highest occupied molecular orbital (E_{HOMO}), lowest unoccupied molecular orbital (E_{LUMO}), energy gap (ΔE), ionization potential (I), electron affinity (A), electronegativity (χ), global hardness (η), global softness (σ), chemical potential (μ), global electrophilicity (ω), electron-accepting (ω^{+}) power, electron-donating (ω^{-}) power, net electrophilicity ($\Delta\omega^{\pm}$), fraction of transferred electrons (ΔN), energy from inhibitor to metals ($\Delta\psi$), and back donation ($\Delta E_{back\text{-}donation}$). These parameters are defined by the following relationships (3–16):

$$I = -E_{HOMO} \quad (3)$$

$$A = -E_{LUMO} \quad (4)$$

$$\Delta E = E_{LUMO} - E_{HOMO} \quad (5)$$

$$\chi = \frac{(I + A)}{2} \quad (6)$$

$$\eta = \frac{(I - A)}{2} \tag{7}$$

$$\mu = \frac{-(I + A)}{2} \tag{8}$$

$$\sigma = \frac{1}{\eta} \tag{9}$$

$$\omega = \frac{\chi^2}{2\eta} \tag{10}$$

$$\omega^+ = \frac{(I + 3A)^2}{(16 \cdot (I - A))} \tag{11}$$

$$\omega^- = \frac{(3I + A)^2}{(16 \cdot (I - A))} \tag{12}$$

$$\Delta\omega^{\pm} = \left[\omega^+ - (-\omega^-)\right] \tag{13}$$

$$\Delta N = \frac{\chi_{Fe} - \chi_{inh}}{2(\eta_{Fe} + \eta_{inh})} \tag{14}$$

$$\Delta\psi = \frac{(\chi_{Fe} - \chi_{inhibitor})^2}{4(\eta_{Fe} + \eta_{inhibitor})} \tag{15}$$

$$\Delta E_{back\text{-}donation} = -\frac{\eta}{4} \tag{16}$$

Where χ_{Fe} is the work function (4.81 eV·mol^{-1}) of iron surface (Fe (110)) which is reportedly more stable and has a greater stabilization energy and the η_{Fe} is the absolute hardness of iron ($\eta_{Fe} = 0$ eV·mol^{-1}).

2.5. MD/MC simulations

The Forcite module from the MatS package was utilized to carry out a blend of Monte Carlo (MC) and Molecular Dynamics (MD) simulations with the objective of exploring the binding capacity of inhibitor molecules to the iron surface. The simulations were performed in a simulation box employing periodic boundary conditions, with dimensions of 2.73 nm×2.73 nm×1.26 nm, accompanied by a 3.5 nm vacuum layer. For the studied system, the Fe (110) surface with a 7-layer slab comprising 847 atoms was chosen due to its superior stability compared to two other common iron crystallographic configurations[19]. Previous literature has extensively detailed the methodologies of MD simulations [20]. The simulation slab model integrated one inhibitor, 800 water molecules, 10 hydronium ions, and

5 chloride ions. In essence, the COMPASSIII force field [21], in conjunction with the NVT ensemble at a temperature of 295 Kelvin was employed for these simulations, which were executed over a duration of 800 picoseconds using a time step of 1 femtosecond [22].

3. Results and Discussion

3.1. Open circuit potential OCP

The variation of OCP with time in the absence and presence of inhibitors is depicted in Figure 3. Clearly, in a corrosive setting without inhibitors, the Open circuit potential shifts towards positive potentials and stabilizes after an hour of being submerged. On the other hand, the introduction of BTMB and BPMS results in a rise in the free potential as the concentration of BTMB/BPMS increases. This phenomenon can be ascribed to the adsorption of inhibitors onto the metal surface and the formation of an inhibitory layer that protects the metal from corrosive particles.

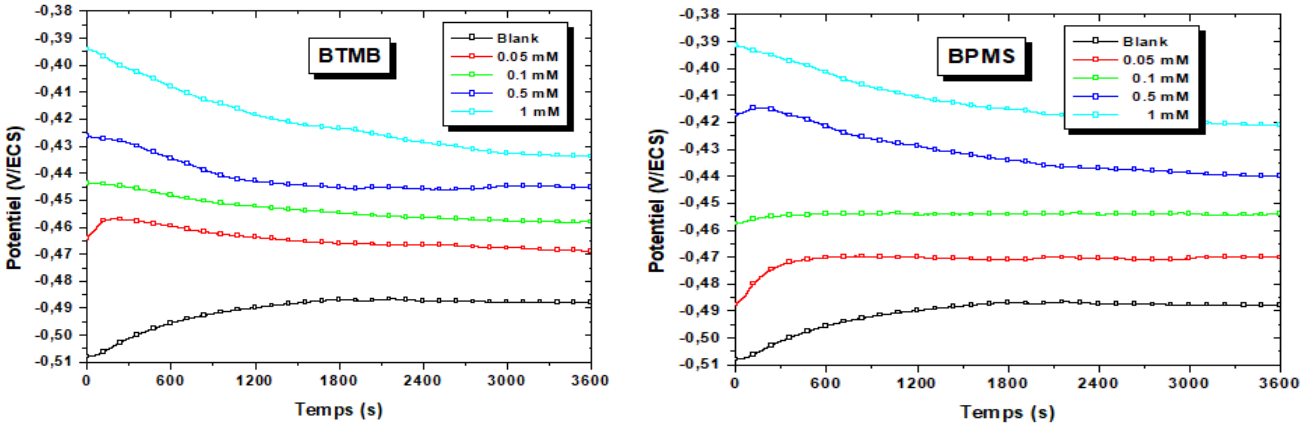

Figure 3. Evolution of the open circuit potential (E_{OCP}) for E24 steel in a 1 M HCl solution with and without BTMB and BPMS over time.

3.2. PDP study

3.2.1. Concentration effect

The polarization curves depicted in Figure 4 elucidate the influence of BTMB and BPMS on the behavior of E24 steel in 1 M HCl across various concentrations. Electrochemical parameters extracted from these curves are summarized in Table 2. The incorporation of BTMB and BPMS effectively mitigates the cathodic hydrogen evolution reaction and attenuates the anodic corrosion of the steel. This is substantiated by a significant reduction in current density and a shift of the corrosion potential towards more positive values. These observed effects can be attributed to the adsorption of inhibitors onto the surface of the substrate [23].

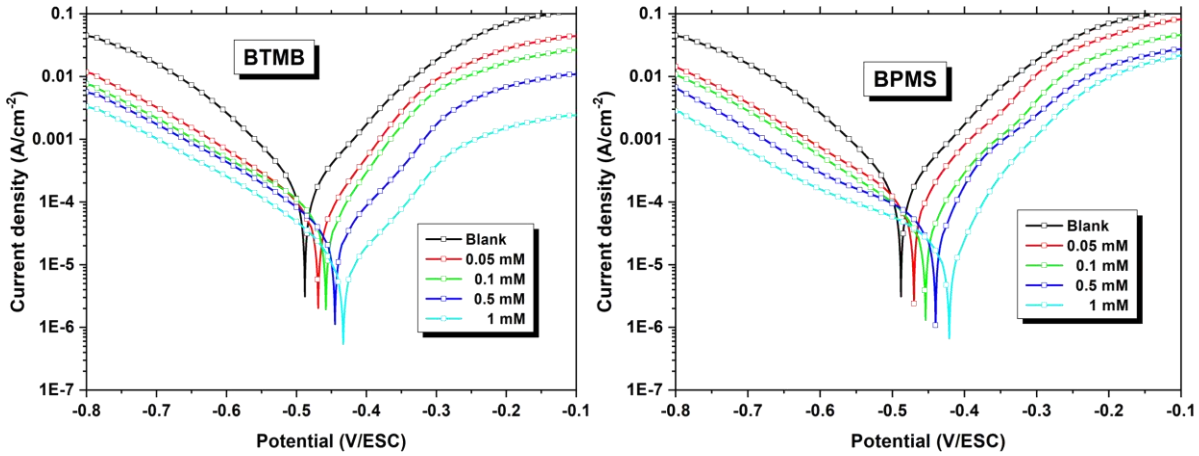

Figure 4. Polarization curves of E24 steel in a 1 M HCl at different concentrations of BTMB and BPMS

Table 2. Electrochemical parameters for E24 in 1 M HCl at various concentrations of BTMB and BPMS.

[C] (mM)	E_{corr} (mV/Ag–AgCl)	i_{corr} (μA/cm^2)	b_c (mV/dec)	b_a (mV/dec)	*IE*%
0	–488	174.8	–94.7	93.3	
		BTMB			
0.05	–469	45.03	–127.5	75.2	74.24
0.1	–458	34.23	–128.8	71	80.42
0.5	–445	24.59	–109.9	84.3	85.93
1	–433	13.41	–119.9	96.9	92.33
		BPMS			
0.05	–470	52.28	–130	61.2	70.09
0.1	–454	32.98	–136.1	68.5	81.13
0.5	–440	29.03	–128.2	44.5	83.39
1	–421	18.58	–93.8	47.3	89.37

Based on the findings acquired (Figure 1 and Table 1), the rise in inhibitor concentration correlates with a decline in current density, accompanied by a subtle shift in the corrosion potential towards less negative values. This trend underscores the inhibitory efficacy of the utilized products in mitigating the corrosion of E24 steel in a 1 M HCl solution. As previously observed, the corrosion current (i_{corr}) diminishes in the presence of inhibitors, leading to an augmented inhibition efficiency (*IE*%). This augmentation reached a maximum of 92.33% and 89.37% for 1 mM of BTMB and BPMS, respectively. This phenomenon is likely attributable to the adsorption of inhibitor molecules onto active sites

on the surface of the E24 steel, forming a protective barrier that delays both anodic and cathodic corrosion reactions at the substrate surface.

3.2.2. Temperature effect

When inhibitors are present or absent, temperature can alter how the E24 steel electrode interacts with acidic media [24] The aim was to assess how changes in temperature affect the inhibition efficiency of BTMB and BPMS, polarization studies were done at temperatures ranging from 293–323 K, without and with 1 mM inhibitors.

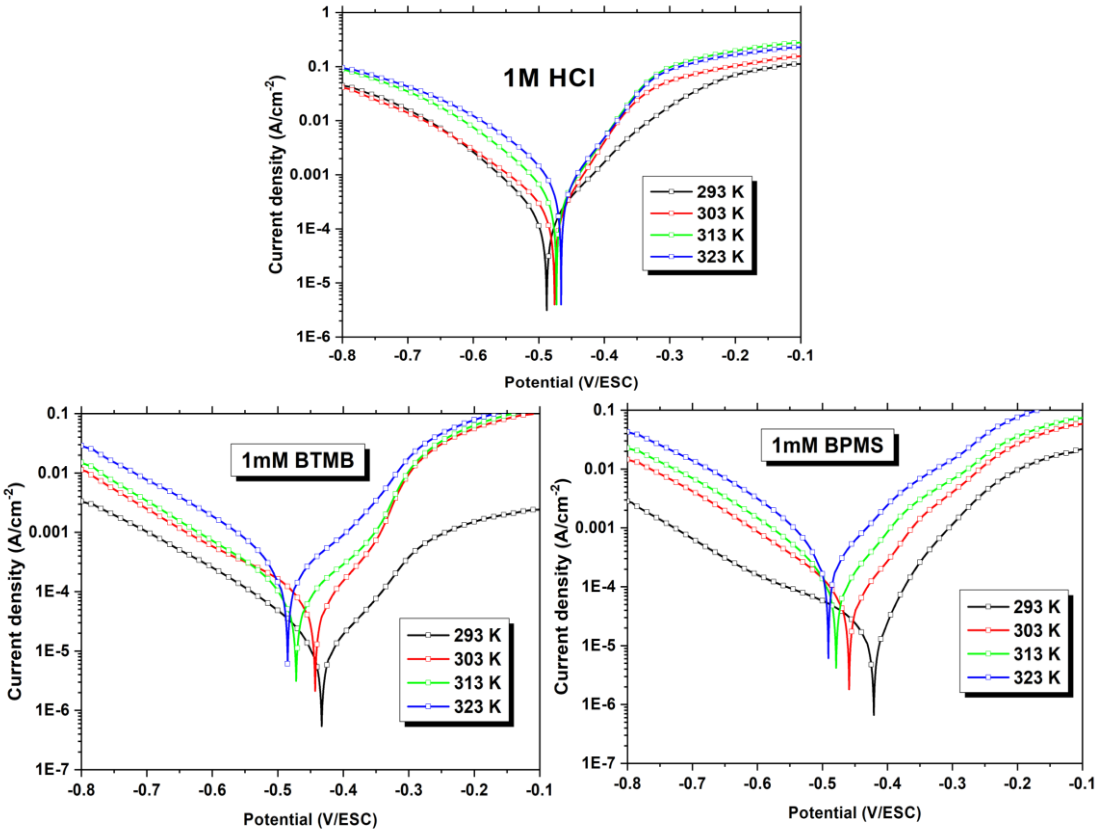

Figure 5. Tafel plots were produced to evaluate the behavior of E24 in a hydrochloric acid solution of 1 mM concentration with and without the addition of 1 mM of BTMB and BPMS at temperatures ranging from 293 K to 323 K.

The findings are presented in Figure 5, while Table 3 provides the corrosion potentials (E_{corr}), corrosion current densities (i_{corr}), and inhibition efficiencies (*IE*%). Analysis reveals that as temperature increases, the corrosion current density also rises, albeit at a slower rate compared to when inhibitors are absent. This indicates a decrease in inhibition efficiency, likely attributed to the adsorption of BTMB and BPMS inhibitors onto the metal surface across all temperatures examined. For instance, the *IE*% values decreased from 92.3% at

293 K to 79.36% at 323 K for BTMB and from 89.37% at 293 K to 74.01% at 323 K for BPMS, respectively. These trends are commonly associated with physical adsorption [25].

Table 3. PDP curves outcomes for E24 steel in a 1.0 M hydrochloric acid (HCl) solution with and without 1 mM of BTMB and BPMS at 293–323 K.

[C] (mM)	T (K)	E_{corr} (mV/Ag–AgCl)	i_{corr} (μA/cm^2)	IE%
0 mM	293	–488	174.8	–
	303	–476	234.7	–
	313	–473	341.7	–
	323	–466	735.6	–
BTMB	293	–433	13.41	92.33
	303	–443	44.45	81.06
	313	–472	65.27	80.89
	323	–485	151.83	79.36
BPMS	293	–421	18.58	89.37
	303	–459	43.33	81.54
	313	–479	74.32	78.25
	323	–491	191.2	74.01

A process of the Arrhenius type, the corrosion reaction's rate is given by (Equation 17) [26]:

$$\ln i_{corr} = \frac{-E_a}{R} \cdot \frac{1}{T} + \ln A \tag{17}$$

The Arrhenius pre-exponential factor, symbolized as A, the universal gas constant, denoted by R, and the apparent activation energy for corrosion, represented by E_a, are utilized to generate Arrhenius plots depicting the corrosion density of E24 steel at a concentration of 1 mM under inhibited and uninhibited conditions, as depicted in Figure 6. Table 4 encapsulates the results obtained from experiments determining the apparent activation energy of corrosion (E_a) for E24 steel in 1 M HCl, both with and without inhibitors, derived from the slopes of $\ln(i_{corr})$ *versus* $1/T$ plots. The data indicate that the presence of inhibitors leads to higher E_a values compared to solutions without inhibitors. This observed increase in E_a values in the presence of inhibitors can be attributed to physical adsorption or weak chemical interactions between inhibitor molecules and the metal surface. These interactions are recognized to heighten the energy barrier for the corrosion process in the presence of inhibitors [27].

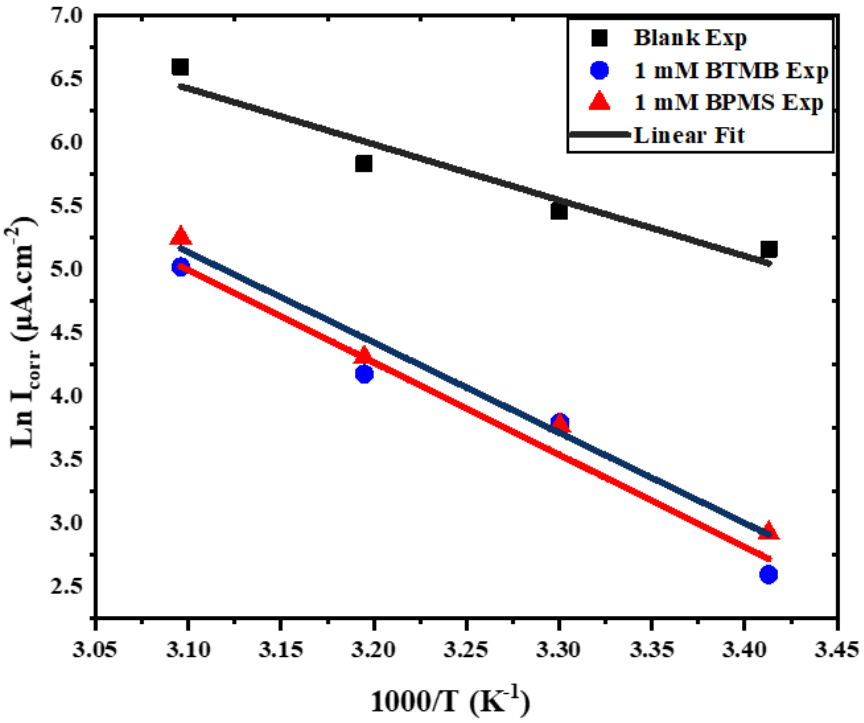

Figure 6. Arrhenius curves were generated for E24 steel in 1 M HCl solution without and with 1 mM of BTMB and BPMS over a temperature range spanning from 293 K to 323 K.

The activation parameters that were computed include enthalpy (ΔH_a) and entropy (ΔS_a) [28]:

$$\ln\left(\frac{i_{corr}}{T}\right) = \frac{-\Delta H_a}{R} \cdot \frac{1}{T} + \ln\left(\frac{R}{Nh}\right) + \frac{\Delta S_a}{R} \tag{18}$$

The activation parameters related to the dissolution process were determined using the entropy (ΔS_a) and enthalpy (ΔH_a), with Planck's constant represented by "h" and Avogadro's number represented by "N". The results are shown in Table 4, which includes the values of ΔH_a and ΔS_a. The Arrhenius plots of Ln(i_{corr}/T) *versus* $1/T$ displayed straight lines with a slope of ($-\Delta H_a/R$) and an intercept of (Ln(R/Nh) + $\Delta S_a/R$), as illustrated in Figure 7. These parameters were used to estimate ΔH_a and ΔS_a values. The positive values of ΔH_a suggested that the E24 steel dissolution process absorbed heat from its surroundings, making it an endothermic process [29]. In addition, the presence of BTMB and BPMS inhibitors causes the standard entropy (ΔS_a), which characterizes the system's unpredictability, to increase, which denotes a spontaneous reaction.

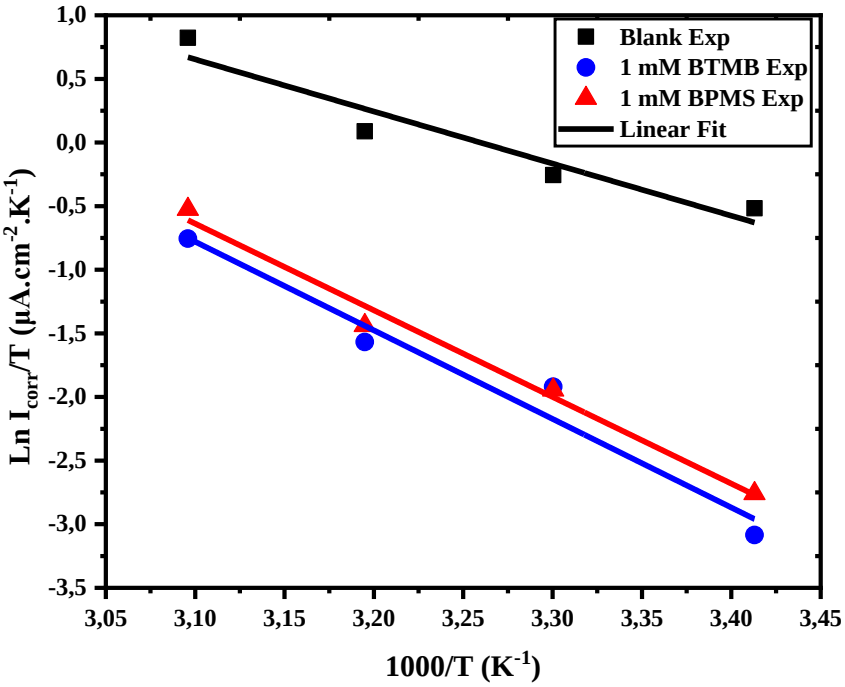

Figure 7. The natural logarithm of i_{corr}/T varied with $1000/T$ at 293–323 K in 1 M HCl without and with the addition of 1 mM of BTMB and BPMS.

The results of the thermodynamic analysis for activating adsorption activity are presented in Table 4, which includes the calculated values of standard activation energy (E_a), enthalpy (ΔH_a), and entropy (ΔS_a) obtained through the use of equations (Equations 17, 18).

Table 4. Activation features of E24 steel corrosion in 1.0 M HCl solution without and with 1 mM of BTMB and BPMS at temperatures ranging from 293 K to 323 K.

Inhibitor	E_a (kJ/mol)	ΔH_a^* (kJ/mol)	ΔS_a^* (J/mol)
Blank	36.61	34.06	–86.53
BTMB	60.45	57.90	–24.53
BPMS	59.19	56.63	–27.27

3.3. Electrochemical Impedance Spectroscopy (EIS)

For a more comprehensive examination of the corrosion prevention mechanism of E24 steel, we have conducted additional analyses including the electrochemical impedance spectrum (Figure 8), as well as the Bode and phase angles (Figure 9).

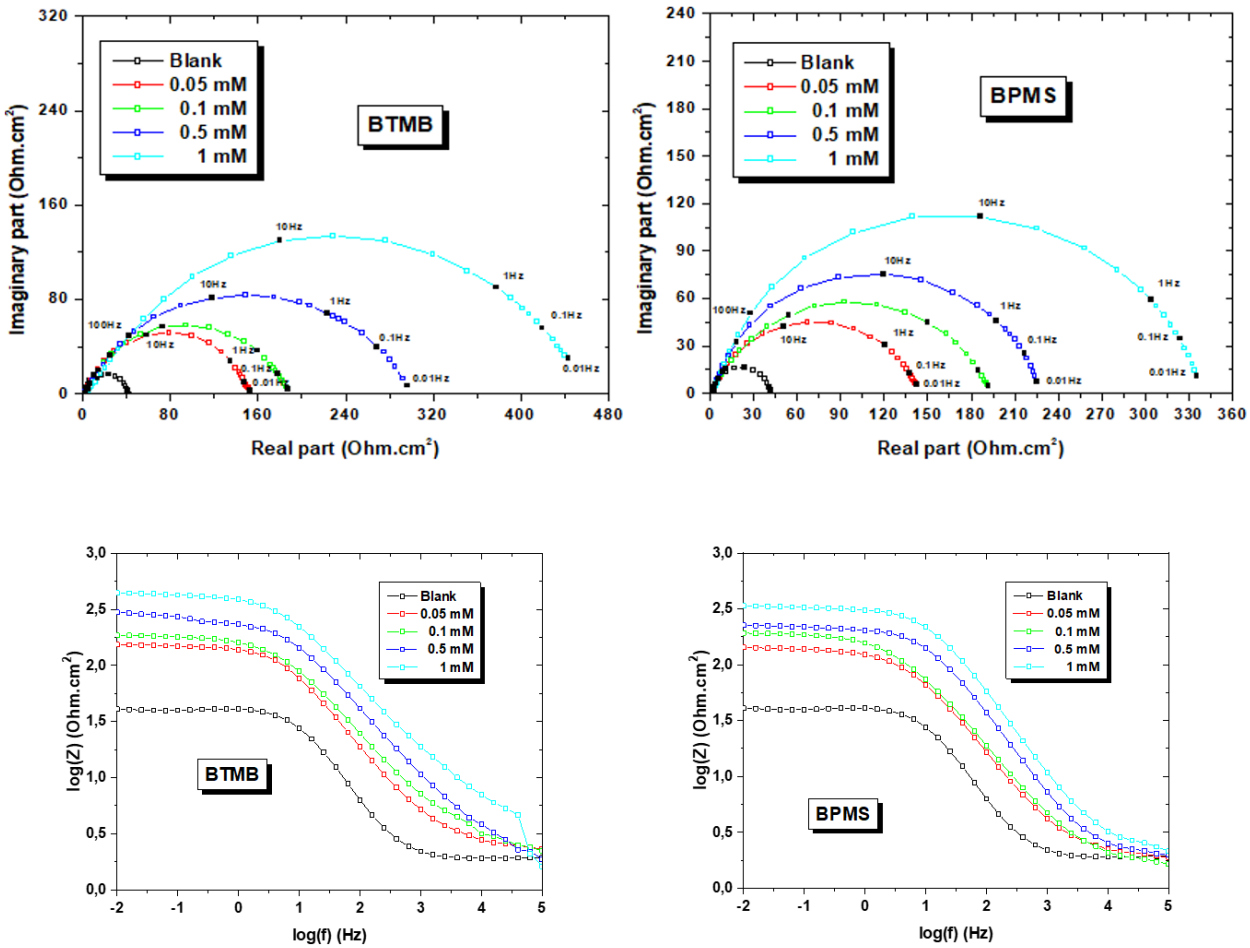

Figure 8. Nyquist plots were obtained for E24 steel in a 1 M HCl solution both in the absence and the presence of BTMB and BPMS.

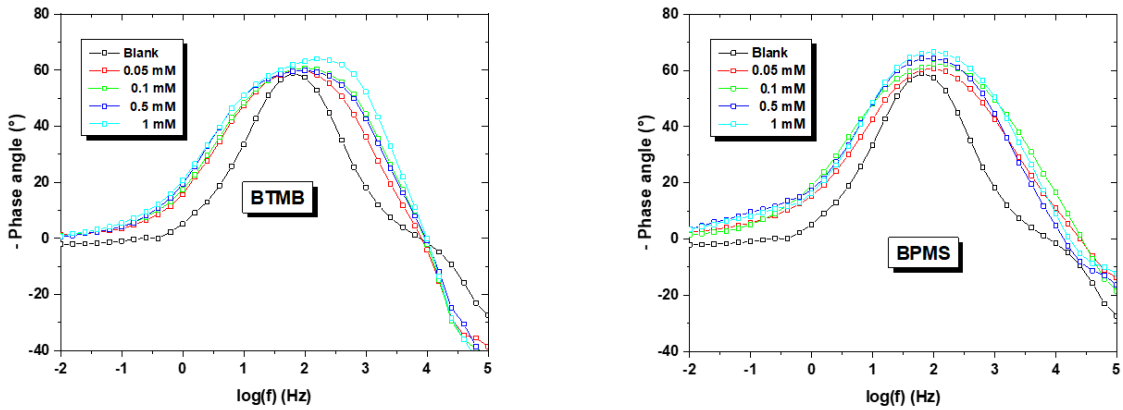

Figure 9. Bode (module (a) / phase (b)) plots were obtained for E24 steel in a 1 M HCl solution both in the absence and in the presence of BTMB and BPMS.

The Nyquist plot exhibited a singular capacitive loop, which expanded in width with increasing concentrations of the two inhibitors. Moreover, the semicircles appeared flattened, indicating a non-ideal capacitive behavior at the electrolyte/metal interface,

potentially attributable to irregularities in the electrode surface [30]. Analysis of the Bode diagrams revealed a solitary time constant, with the protective effects of both inhibitors in acidic solutions exhibiting concentration-dependent trends, as evidenced by the augmented absolute impedance at lower frequencies. Phase angle measurements exceeding 60° underscored the substantial efficacy of both inhibitors [31]. These findings lay the groundwork for further investigation into the corrosion resistance of E24 steel. Phase angle plots across all concentrations unveiled the presence of a singular time constant associated with the charge transfer process. By simulating the Nyquist diagrams using the Ec-Lab program, an equivalent circuit model (see Figure 10) was established. This electrical model integrated the resistance for charge transfer (R_{ct}) and the double-layer capacitance (C_{dl}) in series with the electrolyte resistance, thus facilitating the simulation of impedance diagrams for the electrolyte/metal interface. Parameters derived from the Nyquist diagrams were tabulated in Table 5. The charge transfer resistance (R_{ct}) and solution resistance (R_s) were identified, alongside the inhibition efficiency (*IE*%) and double-layer capacitance (C_{dl}). The tabulated data indicated an inhibition efficiency reaching values of 91.29% and 88.60% at 1 mM concentrations of BTMB and BPMS, respectively. This was supported by a notable increase in charge transfer resistance, rising from 39.67 Ω·cm² in the blank scenario to 455.5 Ω·cm² and 347.98 Ω·cm² for 1 mM BTMB and BPMS concentrations, respectively. Concurrently, the corresponding double-layer capacitance (C_{dl}) decreased from 401.1 μF·cm^{-2} (blank) to 55.21 μF·cm^{-2} (BTMB) and 45.87 μF·cm^{-2} (BPMS). The decline in double-layer capacity could be attributed to either a reduction in the surrounding dielectric constant or an increase in the thickness of the electrical double layer.

Table 5. EIS Measurements of E24 Steel in 1.0 M HCl solution with different concentrations of BTMB and BPMS at 293 K.

[C] (mM)	R_s **(Ω·cm²)**	R_{ct} **(Ω·cm²)**	CPE_{dl} **(μF·cm^{-2})**	***IE*** **(%)**	**θ**
0	1.920	39.67	401.1	–	–
		BTMB			
0.05	1.952	149.8	167.7	73.52	0.7352
0.1	1.892	185.4	135.6	78.60	0.7860
0.5	1.802	297.2	84.61	86.65	0.8665
1	1.798	455.5	55.21	91.29	0.929
		BPMS			
0.05	1.952	142.1	112	72.08	0.7208
0.1	1.810	189.7	83.90	79.09	0.7909
0.5	1.564	225.1	70.70	82.38	0.8238
1	1.047	347.98	45.87	88.60	0.8860

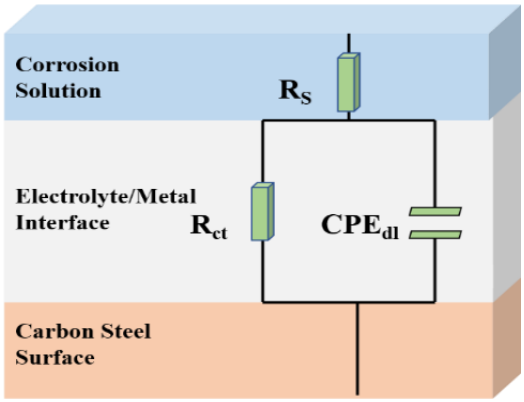

Figure 10. Equivalent electrical circuit with similar functional characteristics.

3.4. Adsorption isotherm

In order to ascertain the nature and potency of the adsorption of BTMB and BPMS inhibitors on E24 steel, the experimental data was matched against different adsorption isotherms, including Temkin, Frumkin, Freundlich and Langmuir. Out of all the adsorption isotherms considered, the Langmuir adsorption isotherm (Figure 11) provided the most precise representation of the inhibitors' adsorption performance [32].

Temkin: $$e^{-2a\theta} = K_{ads} C_{inh} \quad (19)$$

Frumkin: $$\left(\frac{\theta}{1-\theta}\right) e^{-2a\theta} = K_{ads} C_{inh} \quad (20)$$

Freundlich: $$\log\theta = \log K_{ads} + n \log C_{inh} \quad (21)$$

Langmuir: $$\frac{C_{inh}}{\theta} = \frac{1}{K_{ads}} + C_{inh} \quad (22)$$

The term K_{ads} signifies the adsorption equilibrium constant, whereas C_{inh} indicates the inhibitor concentration. The curves showing the fluctuation of C_{inh}/θ in relation to the concentration of C_{inh} for the BTMB and BPMS chemicals are shown in (Figure 11). Table 6 contains the coefficients for the Gibbs free energy of adsorption (ΔG^0_{ads}) calculated from the equation (Equation 23), as well as the K_{ads} measurements obtained by inverting the intercept of the Langmuir isotherm line.

$$K_{ads} = \frac{1}{55.5} \exp\left(-\frac{\Delta G^0_{ads}}{RT}\right) \quad (23)$$

The gas constant is denoted by R and has units of $J \cdot mol^{-1} \cdot K^{-1}$. T is the temperature of the experiment in Kelvin, and the solution has the water concentration of 55.55 (mol/L).

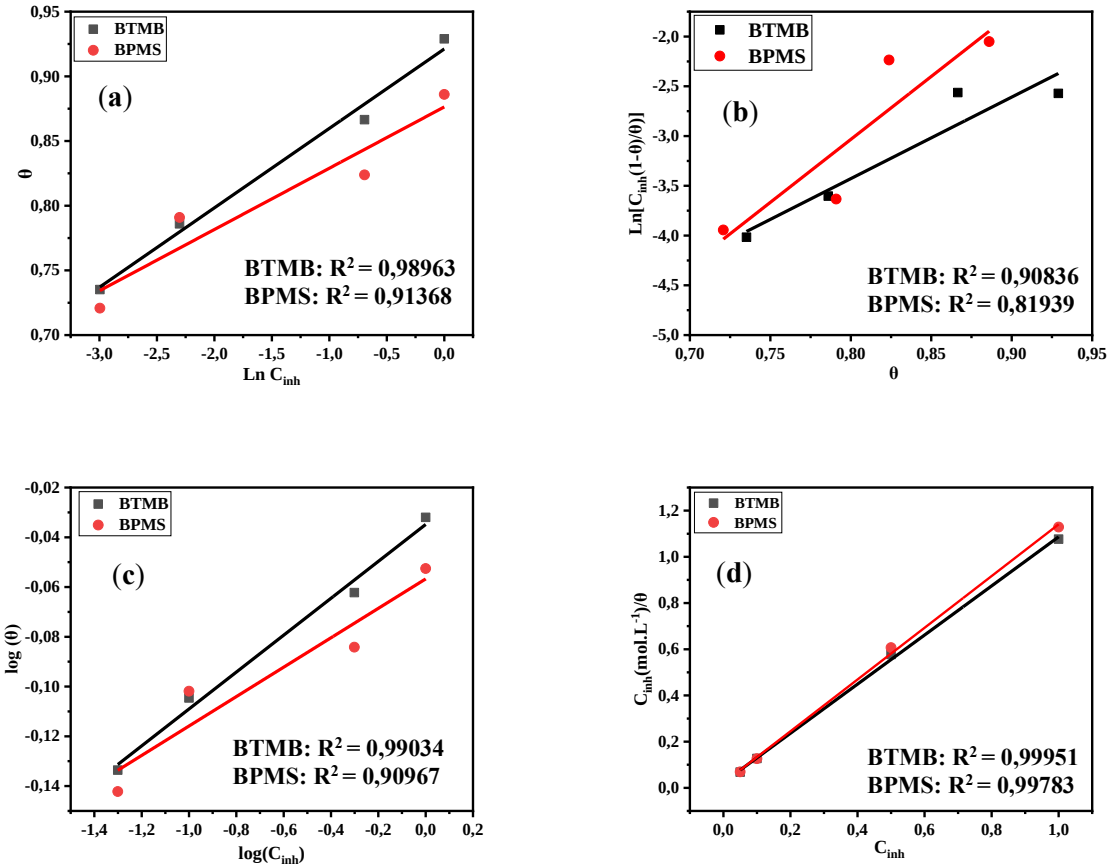

Figure 11. Plots illustrating adsorption isotherms: (a) Temkin, (b) Frumkin, (c) Freundlich, and (d) Langmuir for E24 steel in 1 M HCl of the BTMB and BPMS at different concentrations.

The exceptional adsorption capacity of BTMB and BPMS inhibitors on the surface of E24 steel in 1.0 M acidic HCl was demonstrated by their values of adsorption equilibrium constants, indicating that these inhibitors are best suited for preventing corrosion in locations where it can be most successfully prevented. The fact that the values of ΔG^0_{ads} for BTMB and BPMS are negative (–19.58 kJ·mol^{-1} and –19.54 kJ·mol^{-1}, respectively) indicates that there are spontaneous interactions between the inhibitor molecules and the metal surface [33]. As reported in previous studies, values of ΔG^0_{ads} that are equal to or greater than –20 kJ/mol are typically linked to electrostatic interactions (physisorption) between the sample surfaces and inhibitor. On the other hand, values of ΔG^0_{ads} that are approximately –40 kJ/mol or more negative suggest that the inhibitor and metal surfaces engage in charge sharing (chemisorption). However, in this particular case, the ΔG^0_{ads} values suggest that BTMB and BPMS attach to the E24 steel surface through a physisorption process [34].

Table 6. The adsorption coefficient values (K_{ads}) and the adsorption-free enthalpy (ΔG^0_{ads}) were determined for various concentrations of BTMB and BPMS in 1.0 M HCl.

Inhibitor	K_{ads}, ($mol^{-1} \cdot L$)	R^2	ΔG^0_{ads}, $kJ \cdot mol^{-1}$
BTMB	48.64	0.99951	–19.58
BPMS	47.69	0.99873	–19.54

3.4. DFT considerations

To speed up the computations, a conformer search is performed before the DFT calculations. The search technique is random sampling, the number of conformers is 1000, and the force field used is the COMPASSIII force field (Figure 12).

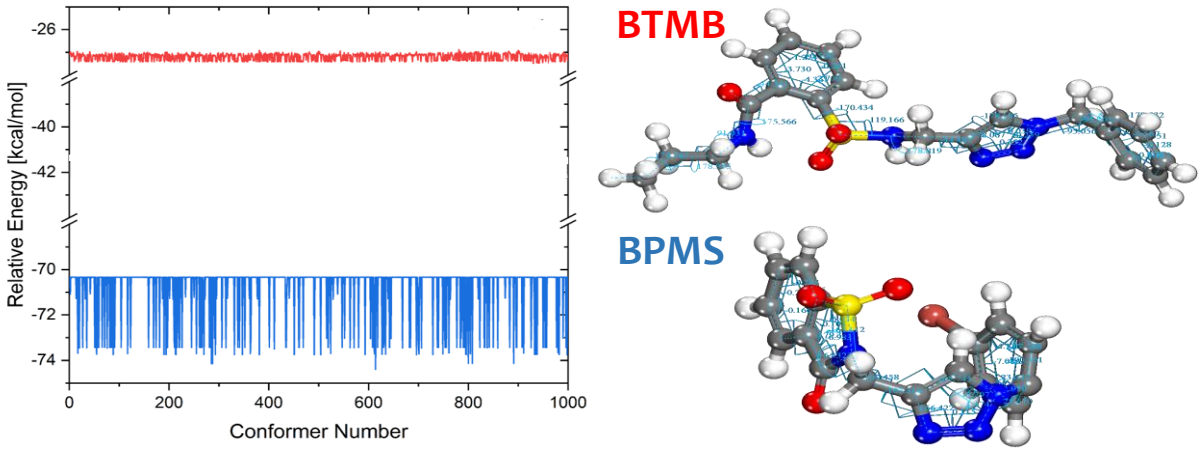

Figure 12. Conformer energy profile search and the resulting lowest energy of BTMB/BPMS.

This research employed density functional theory (DFT) calculations to investigate of the studied inhibitors (BTMB/BPMS) on the metal surface. The Frontier Molecular Orbital (FMO) concept, commonly referred to as FMO theory, is a crucial element in the approach used to determine the chemical properties of corrosion-inhibiting molecules [35].

The Frontier Molecular Orbitals (FMOs) are intimately linked with the energy levels of the lowest unoccupied molecular orbital (LUMO) and the highest occupied molecular orbital (HOMO) within the compound. These orbitals govern the compound's interactions with other molecular species. Prior studies have elucidated that the attachment of corrosion-resistant materials at interfaces occurs *via* a donor-acceptor mechanism [25]. In this mechanism, electron-rich regions of the inhibitor donate electrons to electron-poor regions of the metal (such as the unoccupied d orbitals of Fe atoms), facilitating bonding interactions. Conversely, the inhibitor may also accept electrons from electron-rich regions of the metal (occupied orbitals). The extent of these donor-acceptor interactions, or the degree of interfacial charge-sharing, is dictated by the characteristics of the HOMO and LUMO orbitals [36]. Furthermore, analysis of the HOMO diagram reveals areas of the molecule

predisposed to donating electrons to electrophilic species, while the LUMO diagram highlights regions inclined to accept electrons from nucleophilic species. Figure 13 illustrates a graphical representation of the HOMO and LUMO distributions of a BTMB/BPMS compound obtained through quantum mechanics modeling using the Density Functional Theory (DFT) method [37]. As depicted in Figure 13, for BTMB/BPMS, the HOMO domains are localized predominantly on the ring substituent, whereas the LUMO is distributed over the ring with the sulfonic group. The Molecular Electrostatic Potential (ESP) of the inhibitors was also analyzed to assess their electron density in acidic environments, as shown in Figure 13. This analysis serves to identify regions of high (red, orange, or yellow) or low (blue) electron density within the compound, with green indicating neutral regions [38]. Specifically, the benzene ring, oxygen, sulfur, and nitrogen atoms exhibit high electron density, while low electron density is concentrated around the C and H atoms for BTMB/BPMS. Additionally, employing Mulliken Atomic Charges enables a precise evaluation of the atoms serving as inhibitory sites in the metal adsorption process, which can be inferred from the analysis of Mulliken Atomic Charges (MAC) data. Various hypotheses have been proposed to elucidate the enhanced interaction between specific atoms on the Fe (110) surface and a range of BTMB/BPMS compounds [39]. To elucidate this phenomenon, these hypotheses have been developed, and theoretical frameworks have been constructed to enhance our understanding of these interactions [40]. This phenomenon has garnered considerable attention, with several theories proposed to elucidate and shed light on its underlying mechanisms [41].

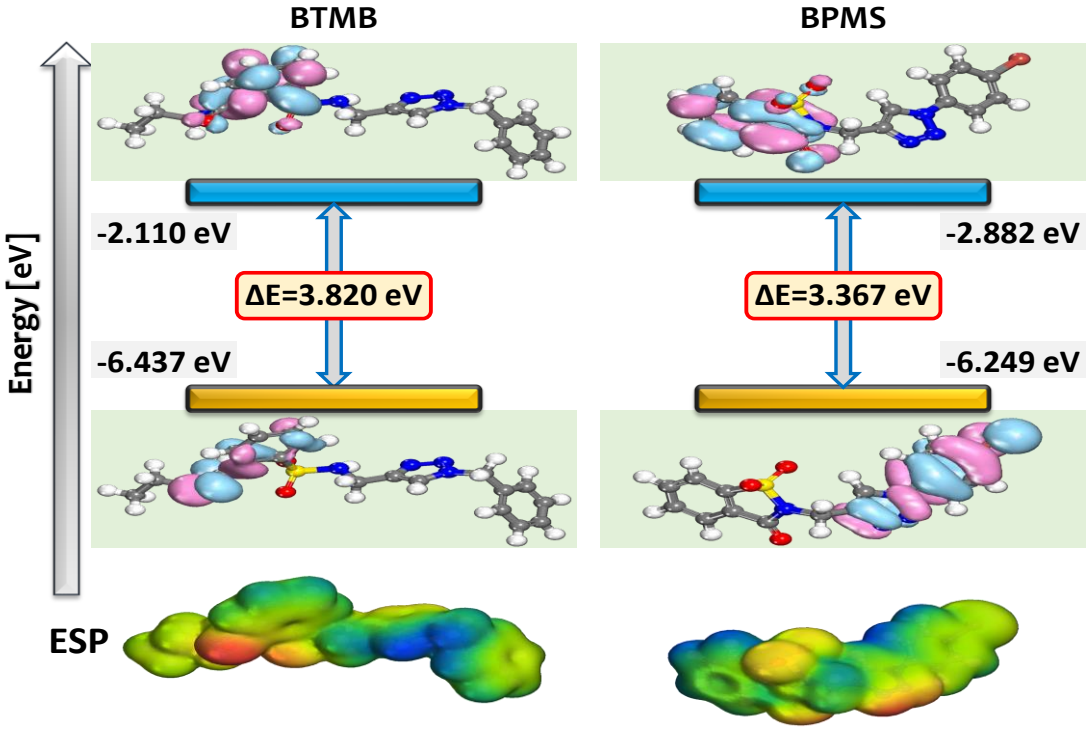

Figure 13. Optimized geometry, HOMO/LUMO and ESP plots of the BTMB/BPMS.

Figure 14. MAC (most negative values) of the BTMB/BPMS.

Table 7 provides the quantum chemical parameters of BTMB and BPMS. Analyzing these descriptors is a practical and recommended approach to improving our understanding of BTMB/BPMS adsorption activities onto metal surface [42].

Table 7. Calculated the theoretical chemical parameters for the BTMB/BPMS.

Descriptor	BTMB	BPMS
E_{HOMO} (eV)	–6.4370	–6.2490
E_{LUMO} (eV)	–2.1100	–2.8820
ΔE (E_{HOMO}–E_{LUMO}) (eV)	4.3270	3.3670
Ionization energy (I) (eV)	6.4370	6.2490
Electron affinity (A) (eV)	2.1100	2.8820
Electronegativity (χ) (eV)	4.2735	4.5655
Global hardness (η) (eV)	2.1635	1.6835
Chemical potential (μ) (eV)	–4.2735	–4.5655
Global softness (σ) (eV^{-1})	0.4622	0.5940
Global electrophilicity (ω) (eV)	4.2207	6.1906
Electron-donating (ω^-) power (eV)	6.6278	8.6838
Electron-accepting (ω^+) power (eV)	2.3543	4.1183
Net electrophilicity ($\Delta\omega^{\pm}$) (eV)	2.2035	4.0031
Fraction of transferred electrons (ΔN) (eV)	–0.2412	–0.3966
Energy from Inhb to Metals ($\Delta\psi$) (eV)	0.1258	0.2649
$\Delta E_{back\text{-}donation}$ (eV)	–0.5409	–0.4209

It is commonly believed that the capacity of BTMB and BPMS to interact with the Fe(110) surface during adsorption is influenced by their capability to exchange electrons. This phenomenon is mostly ascribed to their high ionization potential and low electron affinity [43]. The reason for this is the inhibitors' limited tendency to attract electrons, which

results in their low electron affinity. It is believed that BTMB and BPMS have a profound effect because of the high ionization potential that they possess. This situation arises directly from the inhibitors' substantial electron affinity (Table 7) [44].The chemical structure offers the appearance of being able to donate electrons as well as receive them. It is anticipated that the exchange of lone pair electrons between heteroatoms (O, S, and N) and the unoccupied iron *d*-orbital would result in a slight enhancement of surface adsorption [45]. This is since the lone pair of electrons will be transferred from one to the other. As a consequence of this alteration in the metal, the surface absorption will increase to some degree. There will be an increase in surface adsorption, at least to some degree [46].

3.5. MD/MC simulations

Starting with the Fe(110) surface simplifies the calculation of the system's adsorption energy. Following the completion of MC calculations (Figure 15), a considerable amount of effort was dedicated to investigating the adsorption structure of the BTMB and BPMS to ensure the accuracy of the outcomes [47]. To evaluate the equilibrium state achieved by the MC simulation, the energy values at steady state were compared to those at the beginning of the simulation, and the difference between the two sets of values was calculated. The simulation had advanced to a stage where the system required the minimum energy to continue operating and was operating at its lowest possible energy consumption. The precise arrangement of the active state of adsorbent BTMB/BPMS is depicted in Figure 15.

In the Molecular Dynamics (MD) approach, the BTMB/BPMS molecule adheres to the Fe(110) surface with an orientation that maximizes contact with its oxygen, sulfur, and nitrogen atoms (see Figure 15). This alignment ensures optimal interaction between these atoms and the inhibitor. Our research team suggests that the adsorption pattern illustrated in Figure 15 can be attributed to the binding of the BTMB/BPMS molecule's backbone with the surface atoms of the Fe(110) plane. Substantial evidence supports this hypothesis. BTMB/BPMS molecules exhibit adsorption tendencies, facilitated by their ability to draw their heteroatoms (O, S, and N) and electron rings closer to the surface. The adsorption capability of these molecules arises from their capacity to bring their heteroatoms and electron rings into close proximity with the surface [45].

When inhibitors adhere to the metal surface, they induce a notable change in the surface energy (E_{ads}), as depicted in Figure 16. This phenomenon arises from the heightened adsorption energies displayed by the BTMB/BPMS molecules, leading to a robust interaction with the metal surface. Consequently, a protective layer forms on the metal surface, imparting resistance against corrosion and preserving its original integrity. Researchers advocate for Molecular Dynamics (MD) simulations as they offer a more authentic representation of adsorption dynamics. As illustrated in Figure 17, minimal temperature fluctuations observed during the MD simulation validate its successful execution.

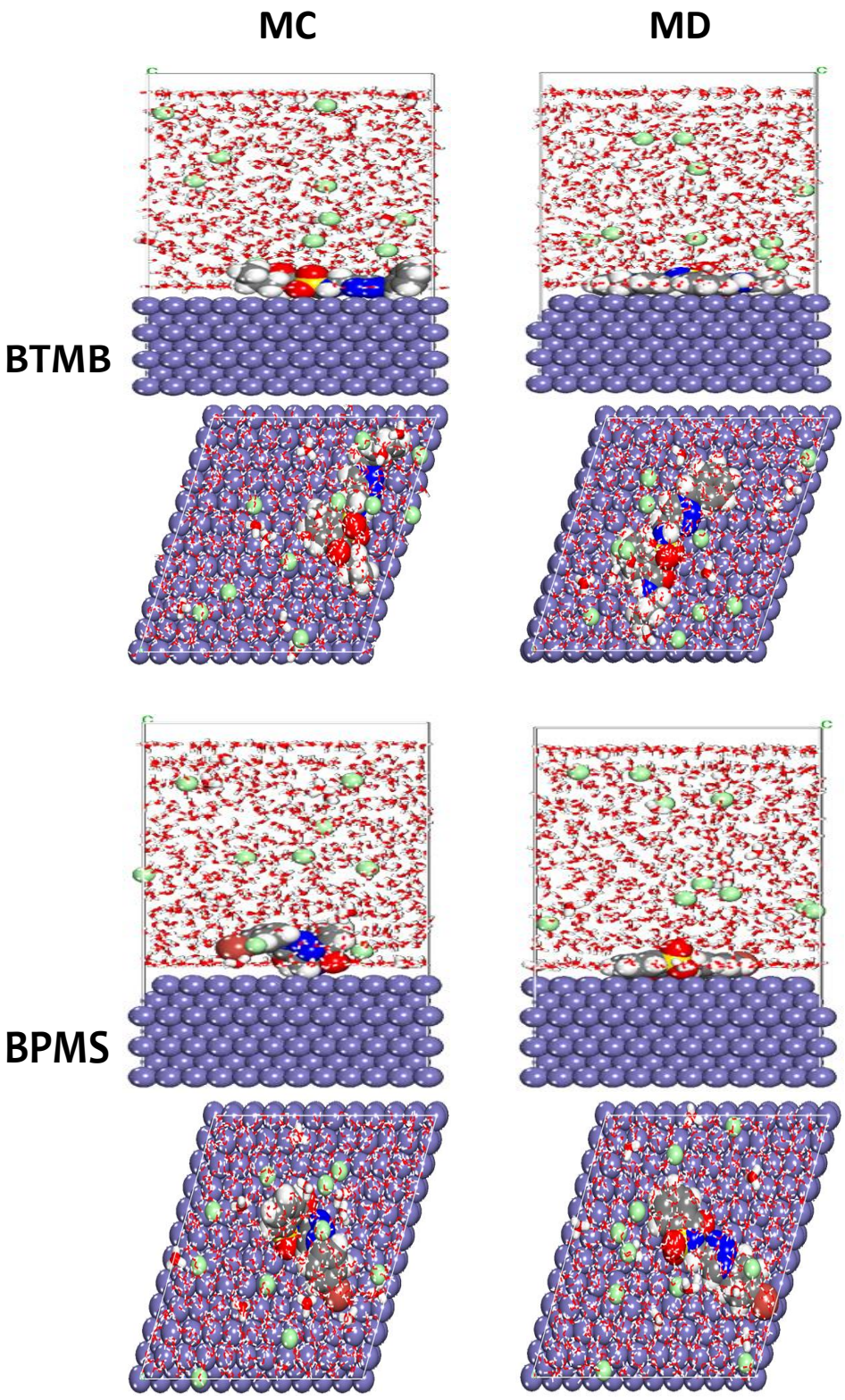

Figure 15. The simulated corrosion media with A. MC and B. MD show minimal BTMB/BPMS adsorption configurations on the Fe (110) substrate.

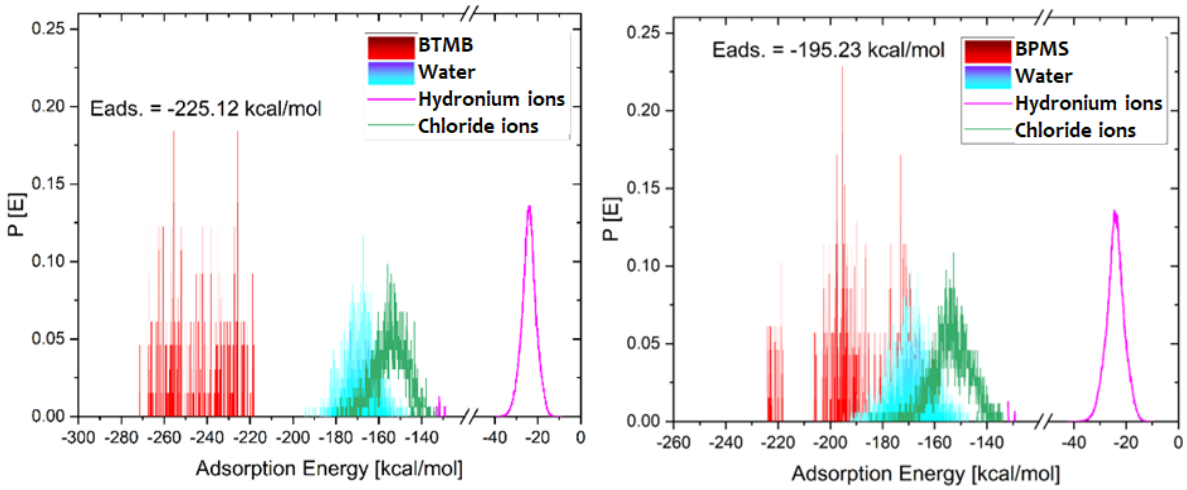

Figure 16. MC calculations were used to obtain the distribution of adsorption energies for the BTMB /BPMS utilized in the simulated corrosion media.

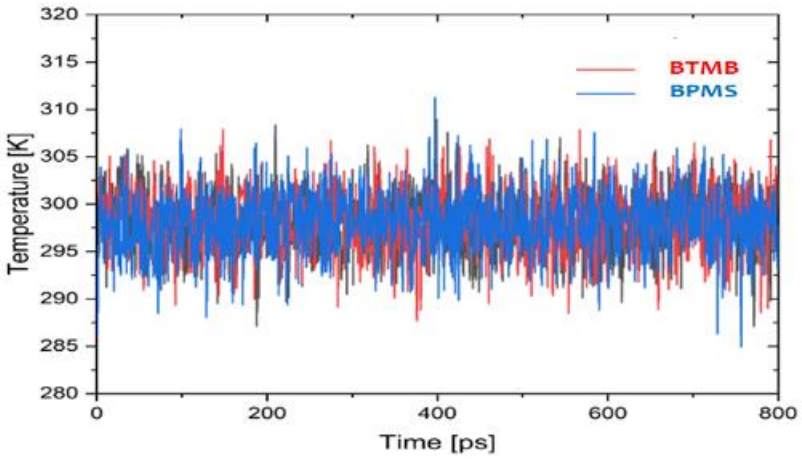

Figure 17. Temperature fluctuations during MD simulation.

The NVT simulation results clearly indicate that the inhibitors depicted in Figure 16 tend to assume a planar configuration along the periphery of the rings upon contact with the metal surface. Upon extending the simulation duration, it became evident that the BTMB/BPMS compounds exhibit robust adherence to the iron surface, suggesting a mechanism for their strong adsorption. Utilizing the radial distribution function (RDF) analysis on the molecular dynamics (MD) trajectory obtained from corrosion simulations represents a reliable and uncomplicated approach to scrutinize the adsorption behavior of corrosion inhibitors on metal surfaces, as outlined in reference. Notably, this analytical method was seamlessly integrated into the simulation process, requiring no intricate procedures[48].

The function that describes the radial distribution is commonly referred to as the RDF, often known as g, is an excellent tool for assessing the interactions between BTMB/BPMS molecules and surfaces in MD simulations (r). As described in references, the peak of the RDF for chemisorption occurs within the range of 1 to 3.5 Å, whereas the peak for

physisorption occurs beyond 3.5 Å [49]. Figure 17 displays the radial distribution function of the BTMB/BPMS, which indicates that the BTMB/BPMS is located at a distance from the Fe (surface) that is less than 3.5 Å. The BTMB/BPMS exerts a significant interaction on the metal surface during contact, as evidenced by the highly negative energy value and the peaks in the RDF. According to the RDF graph, the inhibitor interacts primarily with the iron atoms through the incorporation of oxygen, nitrogen, and sulfur atoms.

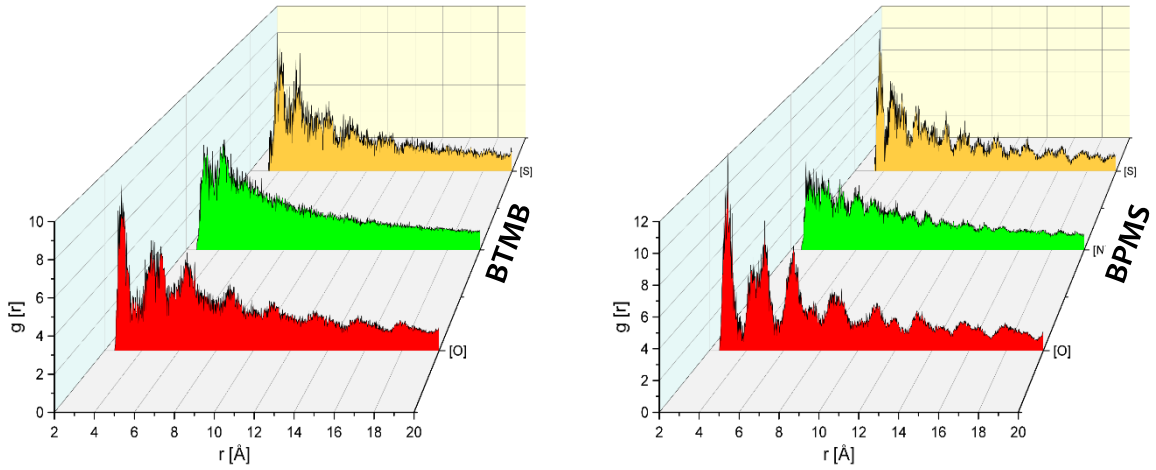

Figure 18. The analysis of the MD trajectory allowed for the determination of the RDF of oxygen, nitrogen, and sulfur atoms of the BTMB/BPMS on the Fe (110) surface.

4. Conclusion

The study's conclusions enable the following inferences:

- According to electrochemical techniques, BTMB and BPMS compounds are effective inhibitors that aid in preventing corrosion of E24 steel in an acidic media
- Polarization studies indicate that BTMB and BPMS exhibit inhibitory characteristics that are of a mixed nature.
- Electrochemical impedance investigations verified the polarization results and showed that BTMB had a better inhibitory efficiency than BPMS.
  The investigation of the impact of temperature on inhibitory effectiveness demonstrates that it decreases as the temperature rises, confirming that the adsorption of the inhibitor molecules on the substrate surface is achieved *via* physical adsorption.
- DFT investigations strongly explore the active adsorption sites of BTMB and BPMS compounds.
- The findings from the MD/MC simulations suggest that the inhibitors adopt a somewhat flat-adsorbed structure on the metal surface which optimizes the interaction with oxygen, nitrogen and sulfur atoms. This configuration is responsible for the inhibitor's protective surface effect. The experimental results provide further support for the notion that the inhibitor has substantial negative adsorption energies.

Declarations

Ethics approval and consent to participate

The study does not require ethical approval.
The study did not involve any animal or human data or tissue.

Consent for publication

All authors have read and agreed to the published version of the manuscript.

Funding

The authors did not receive support from any organization for the submitted work.

Competing interests

The authors declare they have no conflict of interest.

Author contributions

Miloud Errili: Writing – original draft, Validation, Experimental, Formal analysis, Visualization. **Kawtar Tassaoui:** Investigation, Resources. **Anas Chraka:** Writing – review & editing, Software, Conceptualization (supporting). **Mohamed Damej:** Conceptualization, Writing – review & editing. **Najoua Labjar:** Validation, Resources. **Ayoub El mahmoudi:** Validation, Conceptualization. **Khalid Bougrin:** Investigation, Formal analysis. **Avni Berisha:** Methodology, Resources, Writing – original draft, Software. **Mohammed Benmessaoud:** Supervision, Writing – review & editing, Investigation, Methodology, Conceptualization.

Data availability

The datasets generated and/or analyzed during the current study are available from the corresponding author on reasonable request.

References

1. M. Damej, M. Abouchane, M. Doubi, H. Erramli, M. Benmessaoud and N. Hajjaji, Electrodeposition and characterization of poly 3-amino-1,2,4-triazole-5-thiol films on brass electrode in 0.1 M methanol, *Coatings*, 2022, **12**, no. 11, 1784. doi: 10.3390/coatings12111784
2. F. Bouhlal, A. Mazkour, H. Labjar, M. Benmessaoud, M. Serghini-Idrissi, M. El Mahi, El M. Lotfi, S. El Hajjaji and N. Labjar, Combination effect of hydro-alcoholic extract of spent coffee grounds (HECG) and potassium Iodide (KI) on the C38 steel corrosion inhibition in 1M HCl medium: Experimental design by response surface methodology, *Chem. Data Collect.*, 2020, **29**, 100499. doi: 10.1016/j.cdc.2020.100499

3. A. Molhi, R. Hsissou, M. Damej, A. Berisha, V. Thaçi, A. Belafhaili A, M. Benmessaoud, N. Labjar and S. El Hajjaji, Contribution to the corrosion inhibition of C38 steel in 1 M hydrochloric acid medium by a new epoxy resin PGEPPP, *Int. J. Corros. Scale Inhib*., 2021, **10**, no. 1, 399–418. doi: 10.17675/2305-6894-2021-10-1-23
4. M. Benmessaoud, M.S. Idrissi, N. Labjar, K. Rhattas, M. Damej, N. Hajjaji, A. Srhiri and S. El Hajjaji, Inhibition effect of aminotriazole derivative on the corrosion of Cu-40Zn alloy in 3% NaCl solution in presence of Sulphide ions, *Pharma Chem*., 2016, **8**, 122–132.
5. A.M. Nassar, N.S. Ahmed, R.I. El-shazly and Y.K. Abd El Menem, Preparation and evaluation of the mixtures of sulfonate and phenate as lube oil additives, *Int. J. Ind. Chem*., 2017, **8**, 383–395. doi: 10.1007/s40090-017-0128-x
6. A. Dehghani, G. Bahlakeh, B. Ramezanzadeh and M. Ramezanzadeh, Potential of Borage flower aqueous extract as an environmentally sustainable corrosion inhibitor for acid corrosion of mild steel: Electrochemical and theoretical studies, *J. Mol. Liq*., 2019, **277**, 895–911. doi: 10.1016/j.molliq.2019.01.008
7. C. Verma, M.A. Quraishi and E.E. Ebenso, Microwave and ultrasound irradiations for the synthesis of environmentally sustainable corrosion inhibitors: An overview, *Sustainable Chem. Pharm*., 2018, **10**, 134–147. doi: 10.1016/j.scp.2018.11.001
8. M. Errili, A. Al Maofari, K. Tassaoui, M. Damej, Z. Lakbaibi, A. Et-Tahir, S. El Hajjaji and M. Benmessaoud, Electrochemical and theoretical (DFT, MC, MD) evaluation of a new compound based on mercaptobenzimidazole against corrosion of Cu–30Ni in a 3% NaCl solution, *Int. J. Corros. Scale Inhib*., 2023, **12**, no. 2, 458–476. doi: 10.17675/2305-6894-2023-12-2-5
9. A. Chraka, I. Raissouni, N.B. Seddik, S. Khayar, A.I. Mansour, S. Tazi, F. Chaouket and D. Bouchta, Identification of Potential Green Inhibitors Extracted from *Thymbra capitata* (L.) Cav. for the Corrosion of Brass in 3% NaCl Solution: Experimental, SEM–EDX Analysis, DFT Computation and Monte Carlo Simulation Studies, *J. Bio Tribo Corros*., 2020, **6**, 80. doi: 10.1007/s40735-020-00377-4
10. Z. Lakbaibi, M. Damej, A. Molhi, M. Benmessaoud, S. Tighadouini, A. Jaafar, T. Benabbouha, A. Ansari, A. Driouich and M. Tabyaoui, Evaluation of inhibitive corrosion potential of symmetrical hydrazine derivatives containing nitrophenyl moiety in 1M HCl for C38 steel: experimental and theoretical studies, *Heliyon*, 2022, 8. doi: 10.1016/j.heliyon.2022.e09087
11. D.K. Verma, R. Aslam, J. Aslam, M.A. Quraishi, E.E. Ebenso and C. Verma, Computational Modeling: Theoretical Predictive Tools for Designing of Potential Organic Corrosion Inhibitors, *J. Mol. Struct*., 2021, **1236**, 130294. doi: 10.1016/j.molstruc.2021.130294
12. M. Errili, A. Chraka, M. Damej, A.M. El Mahdi, N. Labjar, A. El Mahmoudi, K. Bougrin, A. Berisha and M. Benmessaoud, An Experimental Investigation Linked Detailed-Level Computer Modeling on the Corrosion Inhibitory Activity of 2-((1-benzyl-1*H*-1,2,3-triazol-4-yl) methyl) benzo (d) isothiazol-3 (2H)-one 1, 1-dioxide on

E24 Steel in a 1 M HCl Environment, *Chem. Afr.*, 2024, 1–21. doi: 10.1007/s42250-024-00977-4

13. A. El Mahmoudi, H. El Masaoudi, H. Tachallait, A. Talha, S. Arshad, R. Benhida, J. Boujemaâ, B. Mohammed and K. Bougrin, Selective silver (I)-catalyzed four-component gram-scale synthesis of novel 1,4-disubstituted 1,2,3-triazole-sulfonamides under heterogeneous catalysis and microwave irradiation in water, *Results Chem.*, 2022, **4**, 100552. doi: 10.1016/j.rechem.2022.100552
14. K. Tassaoui, A. Al-Shami, M. Damej, A. Molhi, O. Mounkachi and M. Benmessaoud, Contribution to the corrosion inhibitors of copper-nickel (Cu-30Ni) in 3% NaCl solution by two new molecules of triazole: Electrochemical and theoretical studies, *J. Mol. Struct.*, 2023, **1291**, 135836. doi: 10.1016/j.molstruc.2023.135836
15. C. Tang, A. Farhadian, A. Berisha, M.A. Deyab, J. Chen, D. Iravani, A. Rahimi, Z. Zhang and D. Liang, Novel Biosurfactants for Effective Inhibition of Gas Hydrate Agglomeration and Corrosion in Offshore Oil and Gas Pipelines, *ACS Sustainable Chem. Eng.*, 2023, **11**, 353–367. doi: 10.1021/acssuschemeng.2c05716
16. N. Nairat, O. Hamed, A. Berisha, S. Jodeh, M. Algarra, K. Azzaoui, O. Dagdag and S. Samhan, Cellulose polymers with β-amino ester pendant group: design, synthesis, molecular docking and application in adsorption of toxic metals from wastewater, *BMC Chem.*, 2022, **16**, 43. doi: 10.1186/s13065-022-00837-7
17. V. Barone and M. Cossi, Quantum Calculation of Molecular Energies and Energy Gradients in Solution by a Conductor Solvent Model, *J. Phys. Chem. A*, 1998, **102**, 1995–2001. doi: 10.1021/jp9716997
18. A. Ouaket, A. Chraka, I. Raissouni, M.A. El Amrani, M. Berrada and N. Knouzi, Synthesis, spectroscopic ($^{13}C/^{1}H$-NMR, FT-IR) investigations, quantum chemical modelling (FMO, MEP, NBO analysis), and antioxidant activity of the bis-benzimidazole molecule, *J. Mol. Struct.*, 2022, **1259**, 132729. doi: 10.1016/j.molstruc.2022.132729
19. M. Rbaa, M. Galai, M. Ouakki, R. Hsissou, A. Berisha, S. Kaya, E. Berdimurodov, B. Lakhrissi and A. Zarrouk, Synthesis of new halogenated compounds based on 8-hydroxyquinoline derivatives for the inhibition of acid corrosion: Theoretical and experimental investigations, *Mater. Today. Commun.*, 2022, **33**, 104654. doi: 10.1016/j.mtcomm.2022.104654
20. M. Alahiane, R. Oukhrib, Y.A. Albrimi, H. Abou Oualid, R. Idouhli, A. Nahlé, A. Berisha, N.Z. Azzallou and M. Hamdani, Corrosion inhibition of SS 316L by organic compounds: Experimental, molecular dynamics, and conceptualization of molecules–surface bonding in H_2SO_4 solution, *Appl. Surf. Sci.*, 2023, **612**, 155755. doi: 10.1016/j.apsusc.2022.155755
21. R.L.C. Akkermans, N.A. Spenley and S.H. Robertson, COMPASS III: automated fitting workflows and extension to ionic liquids, *Mol. Simul.*, 2021, **47**, 540–551. doi: 10.1080/08927022.2020.1808215

22. H. Jafari, E. Ameri, M. Rezaeivala, A. Berisha and J. Halili, Anti-corrosion behavior of two N_2O_4 Schiff-base ligands: experimental and theoretical studies, *J. Phys. Chem. Solids*, 2022, **164**, 110645. doi: 10.1016/j.jpcs.2022.110645
23. K. Tassaoui, M. Damej, A. Molhi, A. Berisha, M. Errili, S. Ksama, V. Mehmeti, S. El Hajjaji and M. Benmessaoud, Contribution to the corrosion inhibition of Cu–30Ni copper–nickel alloy by 3-amino-1,2,4-triazole-5-thiol (ATT) in 3% NaCl solution. Experimental and theoretical study (DFT, MC and MD), *Int. J. Corros. Scale Inhib*., 2022, **11**, no. 1, 221–244. doi: 10.17675/2305-6894-2022-11-1-12
24. S. Rekkab, H. Zarrok, R. Salghi, A. Zarrouk, L. Bazzi, B. Hammouti, Z. Kabouche, R. Touzani M. Zougagh, Green Corrosion Inhibitor from Essential Oil of *Eucalyptus globulus* (Myrtaceae) for C38 Steel in Sulfuric Acid Solution, *J. Mater. Environ. Sci*., 2012, **3**, no. 4, 613–627.
25. J. Haque, V. Srivastava, C. Verma and M.A. Quraishi, Experimental and quantum chemical analysis of 2-amino-3-((4-((S)-2-amino-2-carboxyethyl)-1*H*-imidazol-2-yl) thio) propionic acid as new and green corrosion inhibitor for mild steel in 1 M hydrochloric acid solution, *J. Mol. Liq*., 2017, **225**, 848–855. doi: 10.1016/j.molliq.2016.11.011
26. M. Salah, L. Lahcène, A. Omar and H. Yahia, Study of corrosion inhibition of C38 steel in 1 M HCl solution by polyethyleneiminemethylene phosphonic acid, *Int. J. Ind. Chem*., 2017, **8**, 263–272. doi: 10.1007/s40090-017-0123-2
27. F. Bentiss, M. Lebrini and M. Lagrenée, Thermodynamic characterization of metal dissolution and inhibitor adsorption processes in mild steel/2,5-bis(*n*-thienyl)-1,3,4-thiadiazoles/hydrochloric acid system, *Corros. Sci*., 2005, **47**, 2915–2931. doi: 10.1016/j.corsci.2005.05.034
28. Y. Boughoues, M. Benamira, L. Messaadia and N. Ribouh, Adsorption and corrosion inhibition performance of some environmental friendly organic inhibitors for mild steel in HCl solution via experimental and theoretical study, *Colloids Surf., A*, 2020, **593**, 124610. doi: 10.1016/j.colsurfa.2020.124610
29. H. About, M. El Faydy, F. Benhiba, Z. Rouifi, M. Boudalia, A. Guenbour, H. Zarrok, B. Lakhrissi, H. Oudda, I. Warad and A. Zarrouk, Synthesis, Experimental and Theoretical Investigation of Tetrazole Derivative as an Effective Corrosion Inhibitor for Mild Steel in 1 M HCl, *J. Bio Tribo Corros*., 2019, **5**, 50. doi: 10.1007/s40735-019-0233-9
30. A. Fawzy, M. Abdallah, I.A. Zaafarany, S.A. Ahmed and I.I. Althagafi, Thermodynamic, kinetic and mechanistic approach to the corrosion inhibition of carbon steel by new synthesized amino acids-based surfactants as green inhibitors in neutral and alkaline aqueous media, *J. Mol. Liq*., 2018, **265**, 276–291. doi: 10.1016/j.molliq.2018.05.140
31. Y.E. Aoufir, Y.E. Bakri, H. Lgaz, A. Zarrouk, R. Salghi, I. Warad, Y. Ramli, A. Guenbour, E.M. Essassi and H. Oudda, Understanding the adsorption of

benzimidazole derivative as corrosion inhibitor for carbon steel in 1 M HCl: Experimental and theoretical studies, *J. Mater. Environ. Sci*., 2017, **8**, no. 9, 3290–3302.
32. B. Ould Abdelwedoud, M. Damej, K. Tassaoui, A. Berisha, H. Tachallait, K. Bougrin, V. Mehmeti and M. Benmessaoud, Inhibition effect of N-propargyl saccharin as corrosion inhibitor of C38 steel in 1 M HCl, experimental and theoretical study, *J. Mol. Liq*., 2022, **354**, 118784. doi: 10.1016/j.molliq.2022.118784
33. A. Chaouiki, H. Lgaz, R. Salghi, S.L. Gaonkar, K.S. Bhat, S. Jodeh, K. Toumiate and H. Oudda, New Benzohydrazide Derivative as Corrosion Inhibitor for Carbon Steel in a 1.0 M HCl Solution: Electrochemical, DFT and Monte Carlo Simulation Studies, *Port. Electrochim. Acta*, 2019, **37**, 147–165. doi: 10.4152/pea.201903147
34. Z. Akounach, A. Al Maofari, A. El Yadini, S. Douche, M. Benmessaoud, B. Ouaki, M. Damej and S.EL Hajjaji, Inhibition of mild steel corrosion in 1.0 M HCl by water, hexane and ethanol extracts of pimpinella anisum plant, *Anal. Bioanal. Chem*., 2018, **10**, no. 1, 1506–1524.
35. M. Manssouri, Z. Lakbaibi, M. Znini, Y. El Ouadi, A. Jaafar and L. Majidi, Impact of *Aaronsohnia pubescens* Essential Oil to Prevent Against the Corrosion of Mild Steel in 1.0 M HCl: Experimental and Computational Modeling Studies, *Failure Anal. Prev*., 2020, **20**, 1939–1953. doi: 10.1007/s11668-020-01003-8
36. H. Belcadi, A. Chraka, S. El Amrani, I. Raissouni, A. Moukhles, S. Zantar, L. Toukour and A. Ibn Mansour, Investigation and Valorization of the Moroccan *Salvia Officinalis* L. Essential Oil: Phytochemistry, Potential in Corrosion Inhibition, Antibacterial Activity, and Theoretical Modeling, *J. Bio Tribo Corros*., 2023, **9**, 50. doi: 10.1007/s40735-023-00769-2
37. I. Ahamad, R. Prasad and M.A. Quraishi, Experimental and quantum chemical characterization of the adsorption of some Schiff base compounds of phthaloyl thiocarbohydrazide on the mild steel in acid solutions, *Mater. Chem. Phys*., 2010, **124**, 1155–1165. doi: 10.1016/j.matchemphys.2010.08.051
38. R. Hsissou, Review on epoxy polymers and its composites as a potential anticorrosive coatings for carbon steel in 3.5% NaCl solution: Computational approaches, *J. Mol. Liq*., 2021, **336**, 116307. doi: 10.1016/j.molliq.2021.116307
39. A. Abdeslam, L. Zouhair, M. Znini, M. Mounir and L. Amal, Evaluation of corrosion inhibition and adsorption behavior of 7-isopropyl-4-methyl-4,5,6,7-tetrahydrobenzoisoxazole against carbon steel corrosion in 1 M HCl. Experimental and computational investigations, *Anal. Bioanal. Chem. Res*., 2021, **8**, 113–128. doi: 10.22036/abcr.2020.233677.1509
40. O. Blajiev and A. Hubin, Inhibition of copper corrosion in chloride solutions by amino-mercapto-thiadiazol and methyl-mercapto-thiadiazol: an impedance spectroscopy and a quantum-chemical investigation, *Electrochim. Acta*, 2004, **49**, 2761–2770. doi: 10.1016/j.electacta.2004.01.037
41. A. Boutouil, M.R. Laamari, I. Elazhary, L. Bahsis, H. Anane and S-E. Stiriba, Towards a deeper understanding of the inhibition mechanism of a new 1,2,3-triazole derivative

for mild steel corrosion in the hydrochloric acid solution using coupled experimental and theoretical methods, *Mater. Chem. Phys*., 2020, **241**, 122420. doi: 10.1016/j.matchemphys.2019.122420

42. M.A. Migahed, A.M. Al-Sabagh, E.A. Khamis and E.G. Zaki, Quantum chemical calculations, synthesis and corrosion inhibition efficiency of ethoxylated-[2-(2-{2-[2-(2-benzenesulfonylamino-ethylamino)-ethylamino]-ethylamino}-ethylamino)-ethyl]-4-alkyl-benzenesulfonamide on API X65 steel surface under H_2S environment, *J. Mol. Liq*., 2015, **212**, 360–371. doi: 10.1016/j.molliq.2015.09.032
43. O. Dagdag, Z. Safi, O. Hamed, S. Jodeh, N. Wazzan, R. Haldhar, S.K. Safi, A. Berisha and M. El Gouri, Comparative study of some epoxy polymers based on bisphenolic and aromatic diamines: synthesis, viscosity, thermal properties computational and statistical approaches, *J. Polym. Res*., 2021, **28**, 165. doi: 10.1007/s10965-021-02530-0
44. A. Ouass, M. Galai, M. Ouakki, E. Ech-Chihbi, L. Kadiri, R. Hsissou, Y. Essaadaoui, A. Berisha, M. Cherkaoui, A. Lebkiri and E.H. Rifi, Poly(sodium acrylate) and Poly(acrylic acid sodium) as an eco-friendly corrosion inhibitor of mild steel in normal hydrochloric acid: experimental, spectroscopic and theoretical approach, *J. Appl. Electrochem*., 2021, **51**, 1009–1032. doi: 10.1007/s10800-021-01556-y
45. N.B. Iroha, V.C. Anadebe, N.J. Maduelosi, L.A. Nnanna, L.C. Isaiah, O. Dagdag, A. Berisha and E.E. Ebenso, Linagliptin drug molecule as corrosion inhibitor for mild steel in 1 M HCl solution: Electrochemical, SEM/XPS, DFT and MC/MD simulation approach, *Colloids Surf., A*, 2023, **660**, 130885. doi: 10.1016/j.colsurfa.2022.130885
46. A.S. Fouda, S.A. Abd el-Maksoud, E.H. El-Sayed, H.A. Elbaz and A.S. Abousalem, Effectiveness of some novel heterocyclic compounds as corrosion inhibitors for carbon steel in 1 M HCl using practical and theoretical methods, *RSC Adv*., 2021, **11**, 19294–19309. doi: 10.1039/D1RA03083C
47. R. Idouhli, A. Oukhrib, M. Khadiri, O. Zakir, A. Aityoub, Abouelfida. Understanding the corrosion inhibition effectiveness using *Senecio anteuphorbium* L. fraction for steel in acidic media, *J. Mol. Struct*., 2021, **1228**, 129478. doi: 10.1016/j.molstruc.2020.129478
48. F. Tezcan, G. Yerlikaya, A. Mahmood and G. Kardaş, A novel thiophene Schiff base as an efficient corrosion inhibitor for mild steel in 1.0 M HCl: electrochemical and quantum chemical studies, *J. Mol. Liq*., 2018, **269**, 398–406. doi: 10.1016/j.molliq.2018.08.025
49. S. Abbout, R. Hsissou, D. Chebabe, H. Erramli, Z. Safi, N. Wazzan, A. Berisha, A. Reka and N. Hajjaji, Investigation of Two Corrosion Inhibitors in Acidic Medium Using Weight Loss, Electrochemical Study, Surface Analysis, and Computational Calculation, *J. Bio Tribo Corros*., 2022, **8**, 86. doi: 10.1007/s40735-022-00684-y

♦ ♦ ♦